A MESHFREE-BASED TOPOLOGY OPTIMIZATION APPROACH WITHOUT CALCULATION OF SENSITIVITY

Minh Ngoc Nguyen[1,*] **, Tinh Quoc Bui**[2]

[1]*Duy Tan Research Institute for Computational Engineering (DTRICE),*
Duy Tan University, Ho Chi Minh City, Vietnam
[2]*Department of Civil and Environmental Engineering, Tokyo Institute of Technology,*
2-12-1-W8-22, Ookayama, Meguro-ku, Tokyo 152-8552, Japan
*E-mail: nguyenngocminh6@duytan.edu.vn

Abstract. This paper presents a novel topology optimization approach without calculation of sensitivity for the minimum compliance problems, based on the meshfree Radial Point Interpolation Method (RPIM). Relying on the algorithm of Proportional Topology Optimization (PTO), material is distributed using only information of the objective function (which is the elastic strain energy). Material properties are interpolated by the well-known Solid Isotropic Material with Penalization (SIMP) technique; however the pseudo density (design variables) are not defined on the element center as usually encountered in finite element-based approaches, but on integration points. Since no element exists in meshfree analysis, this would be a natural choice. More importantly, the number of integration points is in general larger than that of elements or that of nodes, resulting in higher resolution of the density field. The feasibility and efficiency of the proposed approach are demonstrated and discussed via several numerical examples.

Keywords: meshfree, RPIM, PTO, topology optimization, non-sensitivity.

1. INTRODUCTION

Given a domain with pre-defined loads and boundary conditions, the task of topology optimization is finding the distribution of material that leads to expected structural performance. Early work on this field can be traced back to that of Bendsoe and Kikuchi [1]. Since then, various numerical approaches have been intensively investigated such as the Solid Isotropic Material with Penalization (SIMP) [2, 3], the evolutionary structural optimization (ESO/BESO) [4, 5], the level set method [6], the phase field method [7], etc. Among them, SIMP is currently the most popular approach due to the ease of implementation.

Commonly, the structural performance is analyzed by the Finite Element Method (FEM) and the pseudo-density (the design variable) is defined element-wise [2, 8]. However, the approach is suffered from many limitations, such as checkerboards, mesh-dependency, local minima [9] and mesh distortion [10]. FEM-based techniques with nodal density (i.e. the pseudo-density is assigned to nodes) were also investigated in Refs. [11, 12]. The advantage is that smoother representation of the density field can be obtained, however computational complexity also increases. To overcome the difficulties caused by standard FEM, the node-based topology optimization have been integrated into meshfree methods such as EFG [10, 13, 14], and RKPM [15, 16]. It is well-known that meshfree analyses offer flexibility in domain discretization as well as high accuracy due to the usual higher-order shape functions. Furthermore, most of the meshfree shape functions are lack of Kronecker delta property. As a result, extra techniques have to be introduced for enforcement of boundary conditions [17].

Most of published works on topology optimization employ sensitivity analysis, i.e. derivatives of objective function and derivatives of constraints with respect to the design variables have to be evaluated. Alternatively, non-sensitivity approaches do not need sensitivity analysis during optimization. Luh et al. [18] proposed a binary Particle Swarm Optimization method, in which the pseudo-density in every element may be either zero or unity, representing voided and solid region. However, this method seems to be much inferior to the sensitivity-based methods [19]. Later, the Proportional Topology Optimization (PTO) was proposed by Biyikli and To [20]. The PTO relies on the idea that the material is distributed into each element, proportionally to the contribution of that element to the total strain energy. A 3D version of PTO with a modification of the material interpolation scheme was recently presented in Ref. [21]. Loosely speaking, in PTO, an element with low value of strain energy will receive less material while more material will be assigned to an element with high value of strain energy. The algorithm GOTICA [22] was introduced based on the concept of cellular automata, i.e., the interaction between a cell with its neighboring cells plays a key role in determination of its pseudo-density value. A version of hybrid cellular automata for topology optimization of multi-scale problems was lately proposed by Jia et al. [23]. Although the number of works on non-sensitivity approaches has increased in the last decade, it is still limited, especially in comparison with the majority of sensitivity-based methods.

In this paper, an incorporation of meshfree Radial Point Interpolation Method (RPIM) [24] and the non-sensitivity PTO is presented for the first time, with the expectation to fuse the advantages of the two. RPIM is one of the rare meshfree methods that possess Kronecker delta property, allowing direct imposition of boundary conditions. It is shown that the design variables can be conveniently defined on integration points, instead of nodes like previous works [10, 13–16]. Furthermore, because PTO is a non-sensitivity method, the complexity related to calculation of sensitivity can be avoided.

The rest of the paper is organized as follows. Right after the Introduction is a brief review on the RPIM in Section **2**. Section **3** is reserved for the RPIM-based Proportional Topology Optimization. Numerical examples are discussed in Section **4**, demonstrating the feasibility and efficiency of the proposed approach. Finally, concluding remarks are given in Section **5**.

2. THE RADIAL POINT INTERPOLATION METHOD (RPIM)

2.1. RPIM shape function

Since its introduction [24], the meshfree RPIM has been intensively investigated for nearly two decades. Let us consider a two-dimensional (2D) elastic domain Ω. An arbitrary function $\mathbf{u}(\mathbf{x})$ (e.g. displacement of point $\mathbf{x}$) defined in a sub-domain $\Omega_{\mathbf{x}} \subseteq \Omega$ can be approximated by RPIM as follows

$$\mathbf{u}(\mathbf{x}) \approx \mathbf{u}^h(\mathbf{x}) = [\mathbf{p}(\mathbf{x})\,\mathbf{M} + \mathbf{R}(\mathbf{x})\,\mathbf{N}]\,\hat{\mathbf{u}}(\mathbf{x}) = \mathbf{\Phi}(\mathbf{x})\,\hat{\mathbf{u}}(\mathbf{x}), \tag{1}$$

where $\mathbf{\Phi}(\mathbf{x}) = \begin{bmatrix} \phi_1(\mathbf{x}) & \phi_2(\mathbf{x}) & ... & \phi_n(\mathbf{x}) \end{bmatrix}$ is the vector of RPIM shape function and $\hat{\mathbf{u}}(\mathbf{x}) = \begin{bmatrix} \mathbf{u}(\mathbf{x}_1) & \mathbf{u}(\mathbf{x}_2) & ... & \mathbf{u}(\mathbf{x}_n) \end{bmatrix}^T$ is the vector of nodal values of function $\mathbf{u}(\mathbf{x})$. Here, n is the number of nodes located within subset $\Omega_{\mathbf{x}}$, which is also known as the support domain of point $\mathbf{x}$ (see Fig. 1). $\mathbf{R}(\mathbf{x}) = \begin{bmatrix} R_1(\mathbf{x}) & R_2(\mathbf{x}) & ... & R_n(\mathbf{x})) \end{bmatrix}$ is the vector of n radial basis functions (RBFs), while $\mathbf{p}(\mathbf{x}) = \begin{bmatrix} p_1(\mathbf{x}) & p_1(\mathbf{x}) & ... & p_m(\mathbf{x}) \end{bmatrix}$ is the vector of m augmented polynomial terms. The existence of augmented polynomial terms is required to avoid singularity [17], however the number of m terms can be chosen by users. In fact, it is recommended that the polynomial terms should be selected to form complete polynomials. In the current work, the six terms for complete second order polynomials in 2D domain are used, i.e. $\mathbf{p}(\mathbf{x}) = \begin{bmatrix} 1 & x & y & x^2 & xy & y^2 \end{bmatrix}$. The calculation of matrices $\mathbf{M}$ and $\mathbf{N}$ was presented in details in the Ref. [17] and thus it is not repeated here.
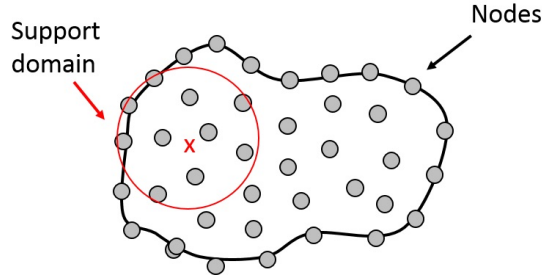

Fig. 1. Illustration of support domain of a point of interest $\mathbf{x}$

There are many types of RBFs such as the multiquadrics, the thin plate splines, the gaussian kernel, etc. [17]. In this paper, the quartic RBF [25] is employed as follows

$$R_i(\mathbf{x}) = 1 - 6\left(\frac{1}{l_s}\right)^2 r_i^2 + 8\left(\frac{1}{l_s}\right)^3 r_i^3 - 3\left(\frac{1}{l_s}\right)^4 r_i^4, \tag{2}$$

in which $r_i = ||\mathbf{x} - \mathbf{x}_i||$ is the distance from node i to the point of interest $\mathbf{x}$. In order to remove the common issue of RBF that accuracy may depend on the choice of shape parameter [25,26], here an adaptive scheme is used. The shape parameter l_s is not set as a pre-defined value but taken as the largest distance between nodes in the support domain of point $\mathbf{x}$. The quartic RBF is thus free from user-defined parameter. The application of this strategy to some other types of RBF can be referred to [25].

2.2. Weak formulation of 2D linear elastic problems

The Galerkin weak formulation of equilibrium equation for a 2D linear elastic body Ω bounded by Γ is given as follow [17]

$$\int_\Omega \delta\boldsymbol{\varepsilon} : \boldsymbol{\sigma}\mathrm{d}\Omega - \int_\Omega \delta\mathbf{u} \cdot \bar{\mathbf{b}}\mathrm{d}V - \int_\Gamma \delta\mathbf{u} \cdot \bar{\mathbf{t}}\mathrm{d}\Gamma = 0, \tag{3}$$

where $\delta\mathbf{u}$ is an arbitrary test function of the displacement $\mathbf{u}$, while $\delta\boldsymbol{\varepsilon}$ is the strain components computed from $\delta\mathbf{u}$. Vector $\bar{\mathbf{b}}$ and $\bar{\mathbf{t}}$ denote the body force and surface force acting on the domain Ω, respectively. The Cauchy stress tensor $\boldsymbol{\sigma}$ is calculated from the Hooke's law by

$$\boldsymbol{\sigma} = \mathbf{C} : \boldsymbol{\varepsilon}, \tag{4}$$

where $\mathbf{C}$ is the fourth order tensor of material properties.

Application of the RPIM method into both the displacement $\mathbf{u}$ and the test function $\delta\mathbf{u}$ read

$$\mathbf{u}(\mathbf{x}) \approx \boldsymbol{\Phi}\hat{\mathbf{u}}, \qquad \boldsymbol{\varepsilon} = \mathbf{B}(\mathbf{x})\hat{\mathbf{u}}, \tag{5}$$

$$\delta\mathbf{u}(\mathbf{x}) \approx \boldsymbol{\Phi}\delta\hat{\mathbf{u}}, \quad \delta\boldsymbol{\varepsilon} = \mathbf{B}(\mathbf{x})\delta\hat{\mathbf{u}}, \tag{6}$$

where $\boldsymbol{\Phi}$ is the vector of RPIM shape function as mentioned above, while matrix $\mathbf{B}$ stores the derivative of shape functions

$$\mathbf{B}(\mathbf{x}) = \begin{bmatrix} \mathbf{B}^1 & \mathbf{B}^2 & ... & \mathbf{B}^n \end{bmatrix}, \quad \mathbf{B}^k = \begin{bmatrix} \dfrac{\partial\phi_k}{\partial x} & 0 \\ 0 & \dfrac{\partial\phi_k}{\partial y} \\ \dfrac{\partial\phi_k}{\partial y} & \dfrac{\partial\phi_k}{\partial x} \end{bmatrix}, \tag{7}$$

in which n is the number of nodes in the support domain of point $\mathbf{x}$. Substitution of Eqs. (4), (5) and (7) into Eq. (3), the following discrete equation is obtained

$$\mathbf{Ku} = \mathbf{F}, \tag{8}$$

where

$$\mathbf{K} = \int_\Omega \mathbf{B}^T \mathbf{C} \mathbf{B}\mathrm{d}\Omega, \tag{9}$$

$$\mathbf{F} = \int_\Omega \boldsymbol{\Phi}^T \bar{\mathbf{b}}\mathrm{d}\Omega + \int_\Omega \boldsymbol{\Phi}^T \bar{\mathbf{t}}\mathrm{d}\Gamma. \tag{10}$$

The above integrals can be conveniently evaluated using numerical integration scheme, e.g.

$$\mathbf{K} \approx \sum_{i=1}^{ng} \mathbf{B}^T(\mathbf{x}_i)\mathbf{C}\mathbf{B}(\mathbf{x}_i)w_i|\mathbf{J}_i| = \sum_{i=1}^{ng} \mathbf{K}_i, \tag{11}$$

where $\mathbf{x}_i$ denotes the coordinates of integration point i; w_i and $|\mathbf{J}_i|$ are the corresponding weights and Jacobian, respectively; and ng is the number of integration points.

3. THE RPIM-BASED PROPORTIONAL TOPOLOGY OPTIMIZATION (RPIM-PTO)

The topology optimization problem for minimum compliance of structures is mathematically stated by

$$\text{minimize } c = \mathbf{u}^T \mathbf{K}(\rho)\mathbf{u}. \tag{12}$$

The above objective function is subject to the following constraints

$$\mathbf{K}(\rho)\mathbf{u} = \mathbf{F}, \tag{13}$$

$$\int_{\Omega} \rho \mathrm{d}\Omega \leq \bar{v} \int_{\Omega} 1 \cdot \mathrm{d}\Omega = \bar{v}|\Omega|, \; \rho \in [0,1]. \tag{14}$$

In fact, the compliance c in Eq. (12) is simply the strain energy being multiplied by two, which can be obtained after solving the equilibrium (see Eq. (13)) for displacement $\mathbf{u}$. The pseudo density field $\rho(\mathbf{x}) \in [0,1]$ is introduced to represent the material distribution, where $\rho = 1$ implies fully solid region and $\rho = 0$ indicates voided region. The constraint in Eq. (14) requires that the volume of the optimized structure should not exceed a pre-defined volume fraction $\bar{v}$ of the design domain. Shortly, the optimization task is to find a layout leading to minimum strain energy, within a certain limited amount of material.

In this work, the design variables (pseudo-density) are defined at integration points. Elastic modulus at an arbitrary integration point i can be interpolated using the solid isotropic material with penalization (SIMP) (see [2,8]) by

$$E_i = E_{void} + \rho_i^p \left(E_s - E_{void} \right), \tag{15}$$

where E_s is the elastic modulus of the solid material, while E_{void} is a small value (e.g. $E_{void} = 10^{-9}$) to avoid zero-stiffness if $\rho_i = 0$. The penalty factor $p = 3$ is chosen in this paper. The stiffness matrix in Eq. (11) is then rewritten by

$$\mathbf{K} \approx \sum_{i=1}^{ng} \mathbf{K}_i, \quad \mathbf{K}_i = \mathbf{B}^T(\mathbf{x}_i)\mathbf{C}(E_i)\mathbf{B}(\mathbf{x}_i)w_i|\mathbf{J}_i|. \tag{16}$$

In a point-based design variable, there exist issues namely "islanding" and "layering" [11], which is similar to the well-known "checkerboards" in element-based approach. Therefore, a density filter is introduced as follows

$$\rho_i = \frac{\sum w_{ij}\hat{\rho}_j}{\sum w_{ij}}, \tag{17}$$

where $\hat{\rho}$ is the non-filtered density. The weights w_{ij} of the filter can be determined by

$$w_{ij} = \begin{cases} \dfrac{r_0 - r_{ij}}{r_0}, & \text{for } r_{ij} \leq r_0 \\ 0, & \text{otherwise.} \end{cases} \tag{18}$$

Here r_{ij} is simply the Euclidean distance between point i and point j, while r_0 is a predefined filter radius.

Based on the Proportional Topology Optimization (PTO) [20,21], no sensitivity analysis is required. Using the evaluation of compliance at every integration point, the pseudo densities are distributed via an inner loop as follows

$$\rho_i = k \frac{c_i}{\sum\limits_{j=1}^{ng} c_j} RM, \tag{19}$$

where RM is the remaining material. The speed of the material distribution process is controlled by coefficient k. It is similar to the "move" parameter in the OC scheme usually used in gradient-based approaches (see [2, 8]). Increasing the value of k may increase the speed of PTO inner loop. However, too large k would lead to non-convergence and violation of the volume constraint. By default, $k = 1$ is selected. At the beginning of the inner loop, RM is set as the target amount of material (see Eq. (14)). The inner loop stops when RM is less than a tolerance, e.g. $RM \leq 10^{-4}$. The evaluation of compliance at integration point is simply calculated by

$$c(\mathbf{x}_i) = \mathbf{u}_{Si}^T \mathbf{K}_i \mathbf{u}_{Si}, \tag{20}$$

where $\mathbf{u}_{Si}$ is the vector of nodal displacement of the nodes belong to the support domain S_i of integration point i. At the end of the inner loop, the pseudo densities are finally updated by

$$\rho_{t+1} = \alpha \rho_t + (1 - \alpha)\rho_{new}, \tag{21}$$

where ρ_t is the density at the last iteration, and ρ_{new} is the newly value obtained after the PTO inner loop. α is a coefficient selected from 0 to 1, exhibiting the weights of history value ρ_t and the calculated value ρ_{new} in ρ_{t+1}. It is obvious that if $\alpha = 1$, there is no update at all; while if $\alpha = 0$, $\rho_{t+1} = \rho_{new}$. In this paper, $\alpha = 0.5$ is chosen.

For meshfree approaches that employ nodal densities [10,13,14], the stiffness matrix is also evaluated using numerical integration (see Eq. (16), in which the value of pseudo density at integration points is interpolated from the nodal values. Since one node may exist in the support domain of many integration points, the calculation of sensitivity is complicated. A nodal integration is then used by [13] to boost computational efficiency, in which the nodes are also integration points. Therefore, it would be straightforward to define the pseudo density on integration points.

It is noted that due to the higher number of integration points, in comparison with that of nodes or that of elements, the RPIM-PTO can be considered as a high-resolution approach. There exist multi-resolution schemes for FEM-based topology optimization, e.g. see Refs. [27,28]. Nevertheless, in those schemes, multi-levels of discretization and extra projection algorithms have to be defined, which are not needed by the RPIM-PTO.

4. NUMERICAL EXAMPLES

4.1. MBB beam

The classical problem of MBB beam is studied in this example to demonstrate the proposed RPIM-PTO. Due to symmetry, half of the design domain is modelled to reduce computational effort. A uniform distribution of 61×31 nodes is employed to discretize

the domain. For numerical integration, 7200 integration points are used. This also means that the pseudo-density field is represented by 7200 design variables. It is noted that for an element-based design scheme using FEM, given the same nodal distribution, there are only 1800 design variables being defined at the center points of 1800 elements. The value of compliance obtained by RPIM is smaller than that of FEM, which is as expected due to the higher number of design variables being used in RPIM.
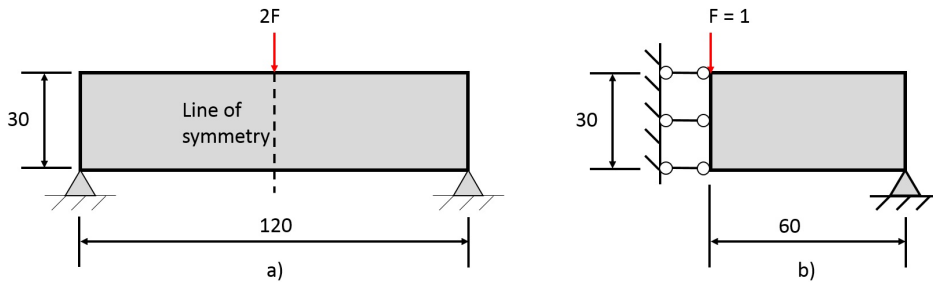

Fig. 2. Design domain of MBB beam problem: a) Full domain and b) Right-half domain

Fig. 3 presents the optimized structure obtained by RPIM-PTO with a volume fraction of 32%. For comparison, the optimized result achieved by FEM-PTO is depicted in Fig. 4. A magnified observation clearly exhibits the higher resolution of the RPIM result, due to the higher number of design variables. The bar graph of elapsed time in Fig. 5 indicates that in order to achieve the same resolution with RPIM-PTO, the FEM-PTO requires
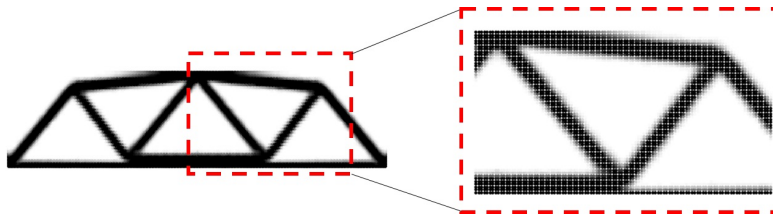
Fig. 3. The optimized result of MBB beam obtained by RPIM-PTO. The pseudo densities are defined at integration points. Value of compliance: $c = 133.43$
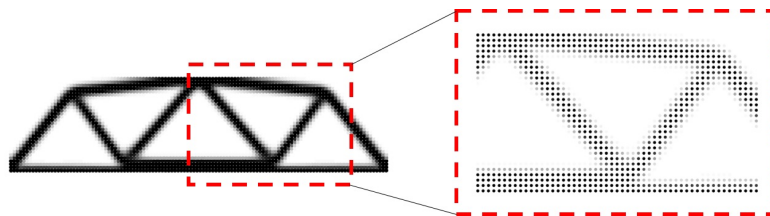
Fig. 4. The optimized result of MBB beam obtained by FEM-PTO, wit. The pseudo densities are defined at element centers. Value of compliance: $c = 140.17$

very high computational cost. Optimized structures with respect to the increasing volume fraction (24%, 32%, 48% and 64%) are portrayed in Fig. 6. The compliance decreases when more materials are retained, as expected. The convergence curves of compliance corresponding to the four cases are depicted in Figs. 7–10.
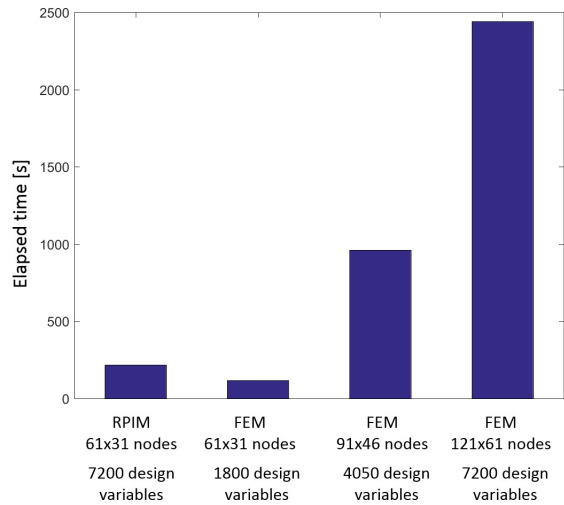

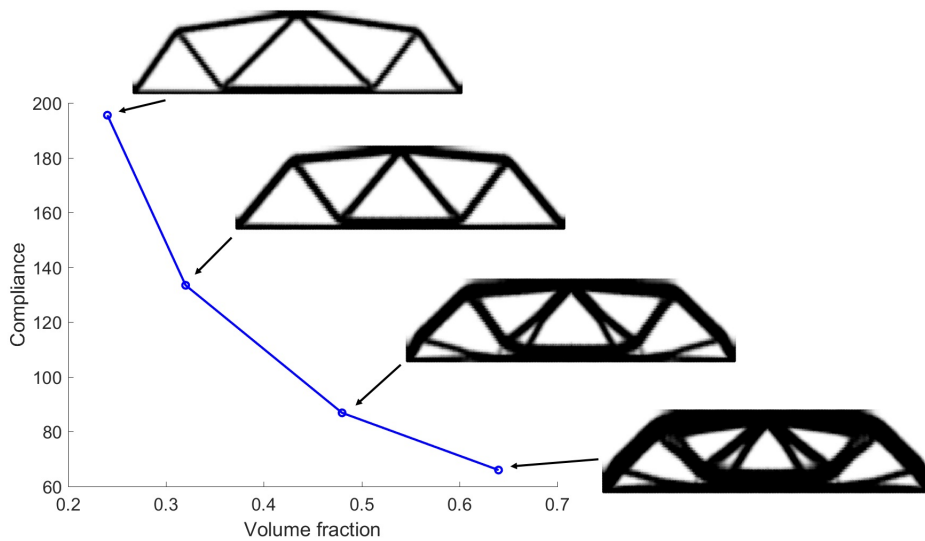*Fig. 5.* Comparison of elapsed time between various schemes

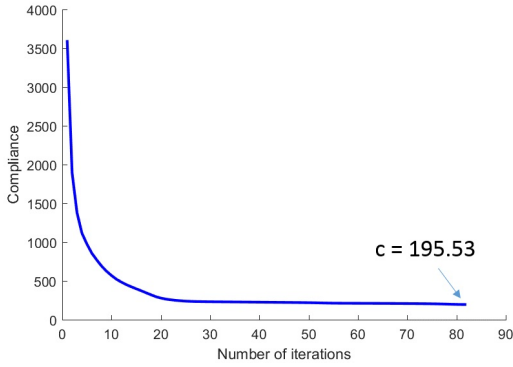*Fig. 6.* Optimized structures with respect to volume fraction

Fig. 7. The convergence history of compliance obtained by RPIM-PTO with volume fraction 24%
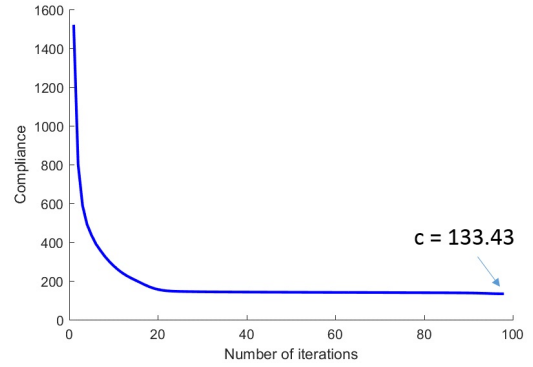
Fig. 8. The convergence history of compliance obtained by RPIM-PTO with volume fraction 32%
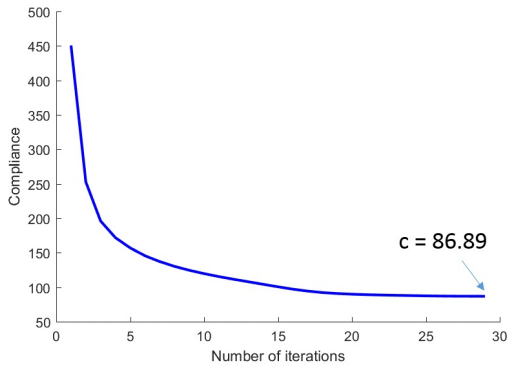

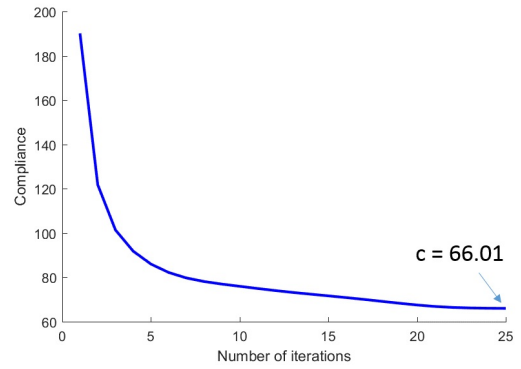Fig. 9. The convergence history of compliance obtained by RPIM-PTO with volume fraction 48%

Fig. 10. The convergence history of compliance obtained by RPIM-PTO with volume fraction 64%

4.2. Annular disc being loaded by tangential loads

In this example, an annular disc being loaded by multiple tangential loads is considered, see Fig. 11. In order to save computational effort, a quarter of the design domain is modelled with anti-symmetric boundary conditions. For numerical analysis, the domain is uniformly discretized by 1681 nodes, while 6400 points are used for numerical integration. Elastic modulus is assumed to vary spatially and thus Eq. (15) is rewritten by

$$E_i = E_{void} + \rho_i^p \left(E_s \exp \left(a \frac{x_i^2 + y_i^2}{R_2^2} \right) - E_{void} \right). \tag{22}$$

The optimized structures obtained for three cases: $a = 0$, $a = -4$ and $a = 4$ are depicted in Fig. 12, Fig. 13 and Fig. 14, respectively. The effect of spatially varying elastic modulus is clearly reflected in the outcomes of topology optimization. In case $a = -4$, the
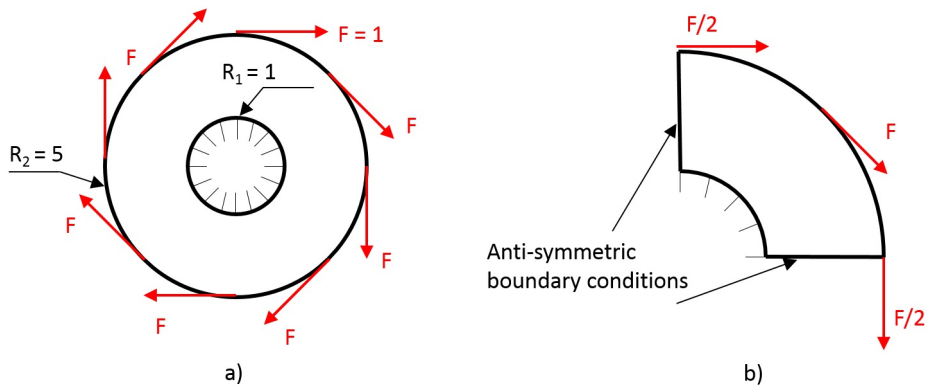
Fig. 11. Geometry of the annular disc being loaded by tangentially loads:
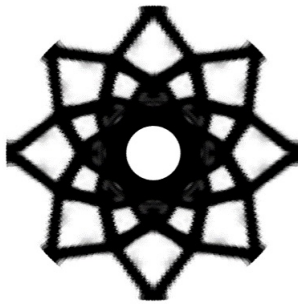a) Full model and b) A quarter model

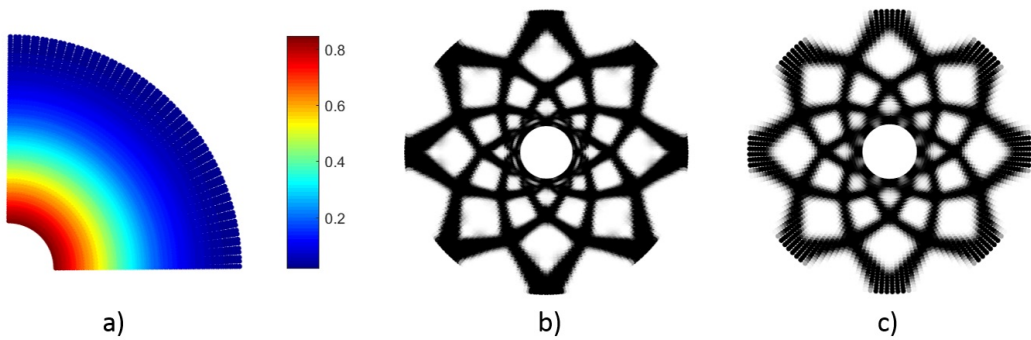*Fig. 12.* Optimized structure in case $a = 0$ (isotropic material)

Fig. 13. a) Distribution of elastic modulus E_s in case $a = -4$, b) The optimized structure by
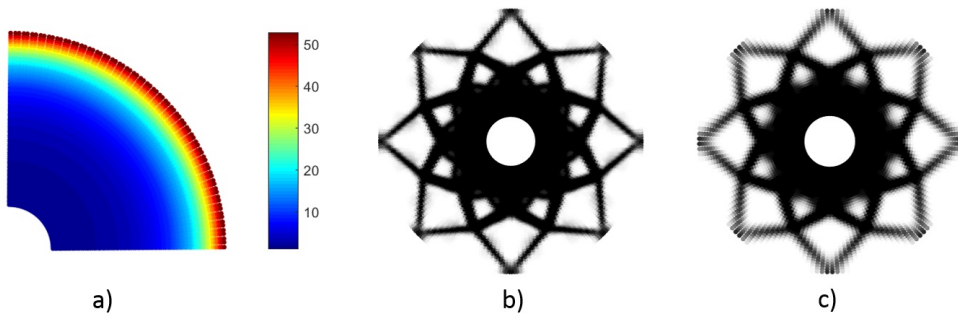RPIM-PTO and c) The optimized structure by FEM-PTO

Fig. 14. a) Distribution of elastic modulus E_s in case $a = 4$, b) The optimized structure by RPIM-PTO and c) The optimized structure by FEM-PTO
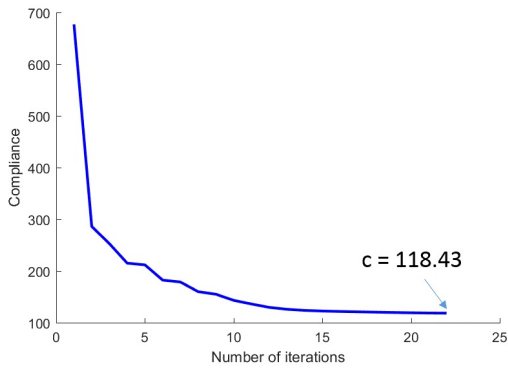

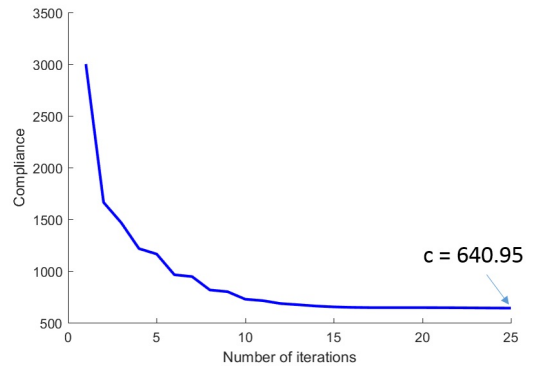*Fig. 15.* The convergence history of compliance obtained by RPIM-PTO for the case $a = 0$ (isotropic material)

Fig. 16. The convergence history of compliance obtained by RPIM-PTO for the case $a = -4$
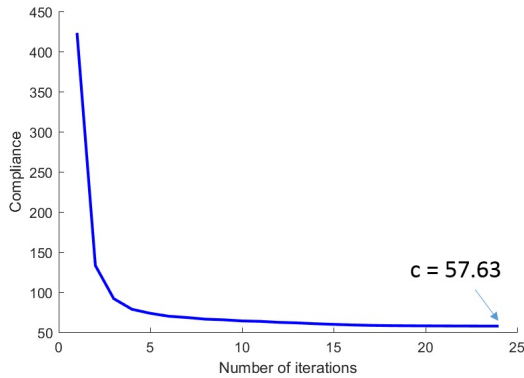

Fig. 17. The convergence history of compliance obtained by RPIM-PTO for the case $a = 4$

material stiffness decreases from inner radius to outer radius. As a result, the structure tends to be thicker near the outer radius. In contrast, in case $a = 4$, the structure is thicker near the inner radius, which is also the region of soft material. Due to lower resolution, the results by FEM-PTO are blurred. The curves showing the convergence of compliance obtained by RPIM-PTO corresponding to the three cases ($a = 0$, $a = -4$, $a = 4$) are exhibited in Figs. 15–17.

5. CONCLUSIONS

The non-sensitivity PTO algorithm has been successfully integrated into meshfree RPIM analysis, namely the RPIM-PTO. The design variables (pseudo-density) are defined at integration points, resulting in a high-resolution scheme with relatively low computational cost. It is emphasized that this is a natural choice by two reasons. Firstly, no element exists in meshfree analysis, hence a point-based density is necessary. Secondly, the evaluation of domain integral (e.g. the structural stiffness) can be conveniently expressed as a sum of values computed at integration points. The part of structural compliance (objective function) associated with each design variable, which is essential in PTO algorithm, is thus straightforwardly calculated.

It is also noted that due to the employment of filter, there exist grey regions, especially near the boundaries. These grey regions cannot be avoided by high-resolution design. In practice, some further treatments [29, 30] should be applied to the design before transferring to the stage of prototype making, e.g. by additive manufacturing.

As a non-sensitivity approach, RPIM-PTO requires no sensitivity analysis. Only the information of the objective function (here is the so-called compliance) is required to update the design variables. Possible extension of the RPIM-PTO would be the problems of compliant mechanism type, and/or structures with large deformation.

REFERENCES

[1] M. P. Bendsøe and N. Kikuchi. Generating optimal topologies in structural design using a homogenization method. *Computer Methods in Applied Mechanics and Engineering*, **71**, (2), (1988), pp. 197–224. https://doi.org/10.1016/0045-7825(88)90086-2.

[2] O. Sigmund. A 99 line topology optimization code written in Matlab. *Structural and Multidisciplinary Optimization*, **21**, (2), (2001), pp. 120–127. https://doi.org/10.1007/s001580050176.

[3] W. Zuo and K. Saitou. Multi-material topology optimization using ordered SIMP interpolation. *Structural and Multidisciplinary Optimization*, **55**, (2), (2016), pp. 477–491. https://doi.org/10.1007/s00158-016-1513-3.

[4] O. M. Querin, G. P. Steven, and Y. M. Xie. Evolutionary structural optimisation (ESO) using a bidirectional algorithm. *Engineering Computations*, **15**, (8), (1998), pp. 1031–1048. https://doi.org/10.1108/02644409810244129.

[5] Y. Tang, A. Kurtz, and Y. F. Zhao. Bidirectional Evolutionary Structural Optimization (BESO) based design method for lattice structure to be fabricated by additive manufacturing. *Computer-Aided Design*, **69**, (2015), pp. 91–101. https://doi.org/10.1016/j.cad.2015.06.001.

[6] M. Y. Wang, X. Wang, and D. Guo. A level set method for structural topology optimization. *Computer Methods in Applied Mechanics and Engineering*, **192**, (2003), pp. 227–246. https://doi.org/10.1016/s0045-7825(02)00559-5.

[7] A. Takezawa, S. Nishiwaki, and M. Kitamura. Shape and topology optimization based on the phase field method and sensitivity analysis. *Journal of Computational Physics*, **229**, (7), (2010), pp. 2697–2718. https://doi.org/10.1016/j.jcp.2009.12.017.

[8] E. Andreassen, A. Clausen, M. Schevenels, B. S. Lazarov, and O. Sigmund. Efficient topology optimization in MATLAB using 88 lines of code. *Structural and Multidisciplinary Optimization*, **43**, (1), (2010), pp. 1–16. https://doi.org/10.1007/s00158-010-0594-7.

[9] O. Sigmund and J. Petersson. Numerical instabilities in topology optimization: A survey on procedures dealing with checkerboards, mesh-dependencies and local minima. *Structural Optimization*, **16**, (1998), pp. 68–75. https://doi.org/10.1007/bf01214002.

[10] Y. Wang, Z. Luo, J. Wu, and N. Zhang. Topology optimization of compliant mechanisms using element-free Galerkin method. *Advances in Engineering Software*, **85**, (2015), pp. 61–72. https://doi.org/10.1016/j.advengsoft.2015.03.001.

[11] S. F. Rahmatalla and C. C. Swan. A Q4/Q4 continuum structural topology optimization implementation. *Structural and Multidisciplinary Optimization*, **27**, (1-2), (2004), pp. 130–135. https://doi.org/10.1007/s00158-003-0365-9.

[12] J. K. Guest, J. H. Prévost, and T. Belytschko. Achieving minimum length scale in topology optimization using nodal design variables and projection functions. *International Journal for Numerical Methods in Engineering*, **61**, (2), (2004), pp. 238–254. https://doi.org/10.1002/nme.1064.

[13] M. Cui, H. Chen, J. Zhou, and F. Wang. A meshless method for multi-material topology optimization based on the alternating active-phase algorithm. *Engineering with Computers*, **33**, (4), (2017), pp. 871–884. https://doi.org/10.1007/s00366-017-0503-4.

[14] J. Zhang, S. Wang, G. Zhou, S. Gong, and S. Yin. Topology optimization of thermal structure for isotropic and anisotropic materials using the element-free Galerkin method. *Engineering Optimization*, **52**, (7), (2019), pp. 1097–1118. https://doi.org/10.1080/0305215x.2019.1636979.

[15] A. Neofytou, R. Picelli, T.-H. Huang, J.-S. Chen, and H. A. Kim. Level set topology optimization for design-dependent pressure loads using the reproducing kernel particle method. *Structural and Multidisciplinary Optimization*, **61**, (5), (2020), pp. 1805–1820. https://doi.org/10.1007/s00158-020-02549-9.

[16] A. Neofytou, T.-H. Huang, S. Kambampati, R. Picelli, J.-S. Chen, and H. A. Kim. Level set topology optimization with nodally integrated reproducing kernel particle method. *Computer Methods in Applied Mechanics and Engineering*, **385**, (2021). https://doi.org/10.1016/j.cma.2021.114016.

[17] G. R. Liu. *Meshfree Methods: Moving Beyond the Finite Element Method*. Taylor and Francis, second edition, (2010).

[18] G.-C. Luh, C.-Y. Lin, and Y.-S. Lin. A binary particle swarm optimization for continuum structural topology optimization. *Applied Soft Computing*, **11**, (2), (2011), pp. 2833–2844. https://doi.org/10.1016/j.asoc.2010.11.013.

[19] O. Sigmund. On the usefulness of non-gradient approaches in topology optimization. *Structural and Multidisciplinary Optimization*, **43**, (5), (2011), pp. 589–596. https://doi.org/10.1007/s00158-011-0638-7.

[20] E. Biyikli and A. C. To. Proportional topology optimization: A new non-sensitivity method for solving stress constrained and minimum compliance problems and its implementation in MATLAB. *PLOS ONE*, **10**, (12), (2015). https://doi.org/10.1371/journal.pone.0145041.

[21] M. N. Nguyen, N. T. Nguyen, and M. T. Tran. A non-gradient approach for three dimensional topology optimization. *Vietnam Journal of Science and Technology*, **59**, (3), (2021), pp. 368–379. https://doi.org/10.15625/2525-2518/59/3/14996.

[22] B. Bochenek and K. Tajs-Zielińska. GOTICA - generation of optimal topologies by irregular cellular automata. *Structural and Multidisciplinary Optimization*, **55**, (6), (2017), pp. 1989–2001. https://doi.org/10.1007/s00158-016-1614-z.

[23] J. Jia, D. Da, C.-L. Loh, H. Zhao, S. Yin, and J. Xu. Multiscale topology optimization for non-uniform microstructures with hybrid cellular automata. *Structural and Multidisciplinary Optimization*, **62**, (2), (2020), pp. 757–770. https://doi.org/10.1007/s00158-020-02533-3.

[24] J. G. Wang and G. R. Liu. A point interpolation meshless method based on radial basis functions. *International Journal for Numerical Methods in Engineering*, **54**, (11), (2002), pp. 1623–1648. https://doi.org/10.1002/nme.489.

[25] T. Q. Bui, N. T. Nguyen, L. V. Lich, M. N. Nguyen, and T. T. Truong. Analysis of transient dynamic fracture parameters of cracked functionally graded composites by improved meshfree methods. *Theoretical and Applied Fracture Mechanics*, **96**, (2018), pp. 642–657. https://doi.org/10.1016/j.tafmec.2017.10.005.

[26] T.-V. Vu, N.-H. Nguyen, A. Khosravifard, M. R. Hematiyan, S. Tanaka, and T. Q. Bui. A simple FSDT-based meshfree method for analysis of functionally graded plates. *Engineering Analysis with Boundary Elements*, **79**, (2017), pp. 1–12. https://doi.org/10.1016/j.enganabound.2017.03.002.

[27] T. H. Nguyen, G. H. Paulino, J. Song, and C. H. Le. A computational paradigm for multiresolution topology optimization (MTOP). *Structural and Multidisciplinary Optimization*, **41**, (4), (2009), pp. 525–539. https://doi.org/10.1007/s00158-009-0443-8.

[28] J. Park and A. Sutradhar. A multi-resolution method for 3D multi-material topology optimization. *Computer Methods in Applied Mechanics and Engineering*, **285**, (2015), pp. 571–586. https://doi.org/10.1016/j.cma.2014.10.011.

[29] T. Zegard and G. H. Paulino. Bridging topology optimization and additive manufacturing. *Structural and Multidisciplinary Optimization*, **53**, (1), (2015), pp. 175–192. https://doi.org/10.1007/s00158-015-1274-4.

[30] K. Zhang and G. Cheng. Three-dimensional high resolution topology optimization considering additive manufacturing constraints. *Additive Manufacturing*, **35**, (2020). https://doi.org/10.1016/j.addma.2020.101224.